



Design and performance study of dry cooling system for 25 MW solar power plant operated with supercritical CO₂ cycle



M. Monjurul Ehsan^{a,*}, Xurong Wang^b, Zhiqiang Guan^a, A.Y. Klimenko^b

^a School of Mechanical and Mining Engineering, The University of Queensland, Brisbane, QLD, 4072, Australia

^b School of Energy and Power Engineering, Xi'an Jiaotong University, Xi'an, Shanxi, 710049, PR China

ARTICLE INFO

Keywords:

Cooling tower
Supercritical CO₂
Heat transfer
Pressure drop
Heat exchanger

ABSTRACT

Dry natural draft cooling towers are mostly employed in thermal power plants in arid areas with no energy consumption and maintenance compared with the mechanical draft cooling system. Different types and shapes of natural draft dry cooling towers (NDDCT) are available in many thermal and nuclear power plant industries. The main purpose of NDDCT is to generate air flow through the finned tube heat exchanger bundles by the influence of buoyancy due to the density difference between the ambient air and the warm air inside the tower. In the present chapter, a one-dimensional MATLAB code is developed to design a NDDCT with detailed specification of finned tube heat exchanger bundles for a 25 MW solar plant operated with supercritical CO₂ (sCO₂) Brayton cycle. The tower height, the tower inlet and outlet diameters and the number of heat exchanger bundles are evaluated after accomplishing the design requirements. The performance study of an air-cooled heat exchanger is performed for a range of sCO₂ inlet temperature from 71 °C to 91 °C, operating pressure from 7.5 MPa to 9 MPa and ambient air temperature from 20 °C to 50 °C. The sCO₂ inlet temperature and operating pressure to the heat exchanger significantly affect the cooling system performance. During high ambient temperature period, the cooling potential of NDDCT is significantly reduced.

1. Introduction

The superior thermo-physical properties and minimal environmental hazards, such as low global warming and ozone depletion, point to CO₂ operated at the supercritical condition as one of the promising refrigerant substitutes in refrigeration and air conditioning technology. Apart from attractive thermodynamic and transport properties (high specific heat and low critical temperature and pressure) of sCO₂, it offers superior safety and economy. CO₂ has been successfully implemented as a working fluid in conventional vapor compression refrigeration cycles and heat pumps for many years. In the last few decades, researchers emphasized exploring the use of sCO₂ as a working fluid in nuclear and thermal power plants. The supercritical CO₂ power cycles are anticipated as one of the next generation power cycles due to lower operation cost and simplified plant design. All thermal power plants need a reliable cooling method to cool the turbine exhaust. The thermal efficiency of any power plant is higher for a higher temperature of the heat source and lower temperature of the heat sink. Therefore, the cooling tower is an essential element of the power plant for efficient operation. The role of a cooling tower is to reject waste heat from the hot working fluid to the atmosphere by means of a cooling medium

such as water or air stream, which are available in abundance. Dry coolers are employed due to water scarcity, low running cost and absence of such environmental issues as water loss, corrosion and scale deposition. NDDCTs are recommended over the mechanical draft due to no parasitic losses associated with fans.

The implementation of sCO₂ in traditional closed-loop Brayton cycle can considerably reduce the compressor work, plant running cost and improve the overall thermal efficiency. It allows the compression process without intercooling, fewer turbine stages and the use of more compact heat exchangers [1]. In the first closed loop, regenerative Brayton cycle was proposed by Feher [2], the compression process was conducted with a pump to handle the high density of sCO₂. Dostal et al. [1] proposed various sCO₂ Brayton cycles and higher efficiency was achieved with recompression Brayton cycle in comparison with helium Brayton cycle. Ma and Turchi [3] suggested the use of sCO₂ both as heat transfer and working fluid in recompression Brayton cycle with thermal storage for concentrating solar power production. To attain a thermal efficiency of more than 50%, Besarati and Goswami [4] proposed different layouts of sCO₂ Brayton cycles with an addition of organic Rankine cycle for proper utilization of waste heat. Chacartegui et al. [5] also observed 7–12% improvement in thermal efficiency by employing

* Corresponding author.

E-mail address: m.ehsan@uqconnect.edu.au (M.M. Ehsan).

Nomenclature			
A	Area, m^2	s	Supercritical
C_p	Specific heat, J/kgK	si	sCO_2 inlet
C_{Dts}	Drag coefficient	so	sCO_2 outlet
D	Hydraulic diameter, m	to	tower outlet
f	Friction factor	ts	tower support
F_T	Correction factor	K	Loss coefficient
F_{Dts}	Drag force, N	l_{ts}	Length of tower support, m
G	Mass velocity, kg/sm^2	L_t	Length of tube, m
H	Height, m	M	Total mass flow rate, kg/s
H	Heat transfer coefficient, W/m^2K	n_{ts}	Number of tower supports
K	Thermal conductivity, W/mK	n_r	Number of tube rows
		n_{tr}	Effective number of tubes per row
		P_f	Fin pitch, m
		P_t	Transversal tube pitch, m
		P_l	Longitudinal tube pitch, m
		P_d	Diagonal tube Pitch, m
		ΔP	Pressure drop, N/m^2
		Q	Heat transfer rate, W
		T	Temperature, $^{\circ}C$ or K
		t_f	Fin thickness (mean), m
		t_{ft}	Fin tip thickness, m
		t_{fr}	Fin root thickness, m
Dimensionless Number		Greek Symbols	
Nu	Nusselt Number	ε	Surface roughness, m
Pr	Prandtl Number	H	Efficiency
Re	Reynolds Number	M	Dynamic viscosity, kg/ms
		P	Density, kg/m^3
		σ	Area ratio
Subscript			
A	air side		
Ct	cooling tower		
Ctc	cooling tower contraction		
Cte	cooling tower expansion		
Cv	control volume		
F	fin		
frT	total frontal		
he	heat exchanger		
pc	Pseudocritical		
r	root		

the combined sCO_2 Brayton and organic Rankine cycle. Garg et al. [6] compared the thermal performance between sCO_2 Rankine cycle and transcritical steam cycle and the proposed sCO_2 Rankine cycle achieved higher efficiency at lower turbine inlet temperature. Dyreby et al. [7] performed modelling study to investigate the influence of operating parameters on the thermal performance of recuperation and recompression sCO_2 Brayton cycles. Yu et al. [8] performed detailed analysis of various thermodynamic cycles for moderate temperature application and energy and exergy analysis were also carried out. A new performance parameter was identified to compare the thermal

performance among various cycles. The authors also [9] conducted a comprehensive review on the performance analysis of various thermodynamic cycles for high temperature application. The influence of various working fluids on the thermal efficiency was also elaborately discussed.

Conboy et al. [10] investigated the influence of turbine and compressor inlet temperatures on the effectiveness of sCO_2 Brayton cycles with dry air-cooled heat exchanger unit. Osorio et al. [11] analyzed the dynamic characteristics of sCO_2 Brayton cycle for a concentrated solar power plant under various seasonal conditions using the forced draft

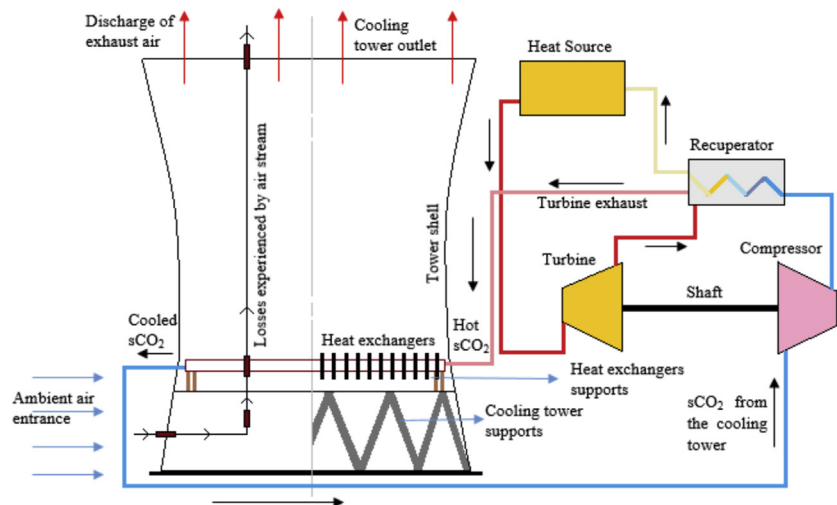


Fig. 1. A typical air-cooled heat exchanger unit to cool sCO_2 in a NDDCT.

dry cooling tower. Singh et al. [12] also performed the influence of solar heat input, mass flow rate, and operating pressure on the net power output of sCO₂ recuperated Brayton cycle coupled with direct dry cooling towers. Padilla et al. [13] employed dry coolers to perform the energy and exergy analysis with four different sCO₂ Brayton cycle configurations. Conradie and Kroger [14] conducted the performance evaluation for both natural draft and mechanical draft cooling towers. Zheng et al. [15] employed solar collector to enhance the thermal effectiveness of a natural draft dry cooling tower. Tanimizu and Hooman [16] performed preliminary numerical and experimental studies with NDDCT, where heat exchanger was arranged in vertical and horizontal configuration.

A number of research studies have explored the possible use of sCO₂ in various Brayton cycle configurations with the natural draft and mechanical draft dry cooling towers. No single study can be found in the literature, which emphasizes the thermal performance analysis of NDDCT operated with sCO₂. In the present article, a validated one-dimensional MATLAB code is generated to design a NDDCT for a 25 MW solar power plant operated with sCO₂ Brayton cycle. The rapid change of thermo-physical properties of sCO₂ in the vicinity of the critical region is well captured by the present code. The changes of various thermodynamic and transport properties along the tube length are taken into account. Finally, the influence of sCO₂ operating temperature and pressure and ambient temperature on the thermal performance of the proposed 25 MW NDDCT are investigated.

2. sCO₂ brayton cycle layout

Fig. 1 demonstrates a typical closed loop sCO₂ Brayton cycle, where sCO₂ exited from the turbine is sent to the recuperator to preheat the compressor outlet sCO₂ stream before entering into the cooling tower. The air-cooled heat exchanger unit transfers the heat from the sCO₂ to the air stream, which flows across the finned tube heat exchanger bundles. Various flow resistances at different sections of a NDDCT are experienced by the air stream and these flow resistances cause a significant pressure drop. The hot air is discharged at a moderate velocity through the outlet of the cooling tower due to the influence of draft force. In the present article, concentration has been paid on the NDDCT. For a 25 MW sCO₂ solar power plant, it has been simulated with software IPSEPro that 49% thermal efficiency can be achieved.

3. Analysis of a NDDCT

Natural draft dry cooling towers (NDDCT) are used in thermal and nuclear power plants. The main task of NDDCT is to produce air flow by means of buoyancy effect. The change of pressure causes the air flow through the outlet of the tower. The hot air inside the tower is lighter than the outside ambient air and a natural draft is produced with the chimney effect. The larger the temperature difference and elevation of the tower, the higher the buoyant force. The volume flow rate of air through the bundles of the heat exchanger is dependent on the temperature difference and the height of tower. The height of the cooling tower can be up to 200 m tall [17]. The arrangement of the heat exchanger bundles can be either horizontal or vertical. In a thermal power plant, natural draft cooling tower can significantly reduce the energy consumption, and cost associated with the maintenance with fans. However, the capital cost for a natural draft cooling tower is much higher than mechanical draft towers. The pressure difference in the tower is a function of different flow resistances experienced by the inlet air while flowing through different sections of the cooling tower [18]. The conservation of energy for a NDDCT can be expressed by the following equation.

The air stream at the entrance of the cooling tower experiences losses (K_{ts}) due to cooling tower support from section 1–2, as shown in Fig. 2. The losses due to cooling tower supports depend on the support length, the number of supports, the width of the support and the

support alignment. Again, losses are encountered by the air stream known as cooling tower inlet loss (K_{ct}) due to the separation of flow, distortion of inlet flow pattern and redirection of air flow. The supports of heat exchangers also exert some losses known as heat exchanger support loss (K_{hes}) from section 2 to section 3. The air stream, while flowing across the finned tube heat exchanger bundles from section 3 to section 4 encounters the following losses, contraction losses (K_{ctc}), expansion losses (K_{cte}) and frictional losses (K_{he}). The flow from section 4 to section 5 is essentially an isentropic flow where the hot air experiences a further loss of kinetic energy, determined by the cooling tower outlet loss coefficient (K_{ct}). In the present work, the various loss coefficients due to flow resistance are evaluated and reported for NDDCT. The corresponding correlations for the loss coefficients are listed in Table 1. By adding all the flow resistances, the total pressure difference between section 1 and 5 is calculated by the following equation, known as the draft equation [19].

$$p_{a1} - \left[p_{a5} + \frac{\left(\frac{m_a}{A_5}\right)^2}{2\rho_{a5}} \right] = (K_{ts} + K_{ct} + K_{hes} + K_{ctc} + K_{he} + K_{cte}) \frac{\left(\frac{m_a}{A_{f34}}\right)^2}{2\rho_{a34}} + p_{a1} \left[1 - \left\{ 1 - 0.00975 \frac{(H_3 + H_4)}{2T_{a1}} \right\}^{3.5} \right] + p_{a4} \left[1 - \left\{ 1 - 0.00975 \left(H_5 - \frac{H_3}{2} - \frac{H_4}{2} \right) T_{a4} \right\}^{3.5} \right]$$

$$Q_a = M_a C_{pa34} (T_{a4} - T_{a3}) = Q_s = M_s C_s (T_{si} - T_{so})$$

$$Q_{hx} = \frac{UA F_T [(T_{si} - T_{a4}) - (T_{so} - T_{a3})]}{\ln \left[\frac{(T_{si} - T_{a4})}{(T_{so} - T_{a3})} \right]}$$

4. Analysis of air cooled heat exchanger

The air-cooled heat exchanger unit transfers the heat from the working fluid to the fresh air stream flowing across the bundles of tubes

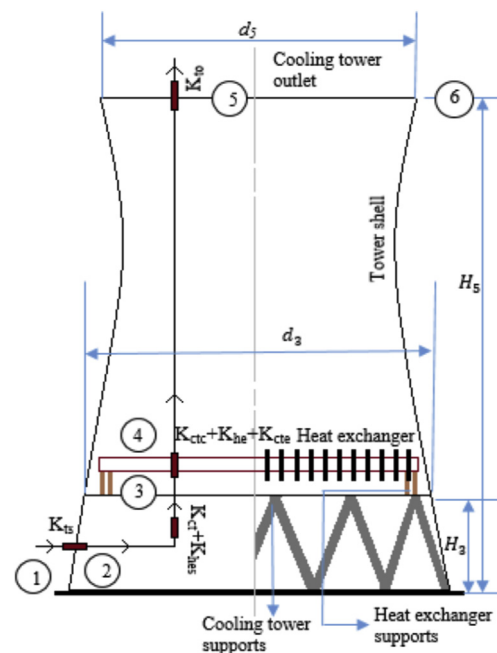


Fig. 2. Definition of various loss coefficients at different parts of a NDDCT.

Table 1
Loss coefficient equations for NDDCT.

Loss Coefficient	Equation
Cooling tower outlet loss coefficient K_{lo} [19]	$K_{lo} = \frac{\Delta p_{a56}}{\rho_{a5} v_{a5}^2} = \frac{2\rho_{a5} \Delta p_{a56}}{\left(\frac{m_a}{A_5}\right)^2} = -0.28 Fr_D^{-1} + 0.04 Fr_D^{-1.5}$ $Fr_D = \left(\frac{m_a}{A_5}\right)^2 / [\rho_{a5}(\rho_{a6} - \rho_{a5})g d_5]$ <p>Valid for $0.5 \leq \frac{d_5}{d_3} \leq 0.85$ and $5 \leq K_{he} \leq 40$</p>
The tower support loss efficient K_{ts} [19]	$K_{ts} = \frac{2\Delta p_{ats}}{\rho_{a1} v_{a2}^2} = \frac{C_{Dis} L_{ts} d_{ts} n_{ts}}{\pi d_3 H_3}$ $\Delta p_{ats} = \frac{\rho_{a1} v_{a2}^2 C_{Dis} L_{ts} d_{ts} n_{ts}}{2\rho_{a1} d_3 H_3}; C_{Dis} = 2Fr_{Dis} / (\rho_{a1} v_{a2}^2 A_{ts})$ <p>Based on the condition of the heat exchanger, tower support loss coefficient,</p> $K_{tshe} = \frac{2\Delta p_{ats} \rho_{a34}}{\left(\frac{m_a}{A_{fr}}\right)^2} = \frac{C_{Dis} L_{ts} d_{ts} n_{ts} A_{fr}^2}{(\pi d_3 H_3)^3} \left(\frac{\rho_{a34}}{\rho_{a1}}\right)$
Contraction loss efficient, K_{ctc} [19]	$K_{ctc} = \left(1 - \frac{2}{s_c} + \frac{1}{s_c^2}\right) \left(\frac{\rho_{a34}}{\rho_{a1}}\right) \left(\frac{A_{fr}}{A_{e3}}\right)^2$
Expansion loss efficient, K_{cte} [19]	$K_{cte} = \left(1 - \frac{A_{e3}}{A_3}\right)^2 \left(\frac{\rho_{a34}}{\rho_{a1}}\right) \left(\frac{A_{fr}}{A_{e3}}\right)^2$
Cooling tower inlet loss coefficient, K_{ct}	$K_{cthe} = K_{ct} (\rho_{a34} / \rho_{a1}) (A_{fr} / A_3)^2$ <p>Terblanche and Kroger [23] correlation,</p> $K_{ct} = \frac{\rho_{a1} - \rho_{a4} + \frac{v_a}{2}}{\frac{\rho_{a3}}{2}} - K_{he} \left(\frac{\rho_{a3}}{\rho_{a34}}\right) \left(\frac{A_3}{A_{fr}}\right)^2$ <p>Based on the condition of the heat exchanger [23],</p> $K_{ct} = \left[100 - 18\left(\frac{d_3}{H_3}\right) + 0.94\left(\frac{d_3}{H_3}\right)^2\right] x K_{he}^{-1.28+0.183\left(\frac{d_3}{H_3}\right) - 7.769 \times 10^{-3}\left(\frac{d_3}{H_3}\right)^2}$ <p>Valid for $10 \leq \frac{d_3}{H_3} \leq 15$, $5 \leq K_{he} \leq 25$ and $\frac{t_s}{d_3} = 0.0045$</p> <p>Preez and Kroger [24] correlation,</p> $K_{ct} = \left[-18.7 + 8.095\left(\frac{d_3}{H_3}\right) - 1.084\left(\frac{d_3}{H_3}\right)^2 + 0.0575\left(\frac{d_3}{H_3}\right)^3\right] x K_{he}^{0.165-0.035\left(\frac{d_3}{H_3}\right)}$ <p>Geldenhuis and Kroger [25] correlation,</p> $K_{ct} = 0.072\left(\frac{d_3}{H_3}\right)^2 - 0.34\left(\frac{d_3}{H_3}\right) + 1.7$ <p>Preez and Kroger [26] correlation,</p> $K_{ct} = \left[1.05 - 0.01\left(\frac{d_3}{H_3}\right)\right] \left[1.6 - 0.29\left(\frac{d_3}{H_3}\right) + 0.072\left(\frac{d_3}{H_3}\right)^2\right] / s_c$ $+ (0.271 - 0.0115K_{he} + 0.000124K_{he}^2) \left(\frac{d_3}{H_3}\right) (1.66 - 6.325s_c + 5.625s_c^2)$ <p>Valid for $5 \leq \frac{d_3}{H_3} \leq 10$, $19 \leq K_{he} \leq 50$ and $0.4 \leq s_c \leq 1$</p> <p>Here, s_c is the ratio of the effective length of heat exchanger along the tower circumference to the tower perimeter.</p> <p>Vauzanges and Ribier [27] correlation,</p> $K_{ct} = 1.5 \exp\left(0.2 \frac{d_3}{H_3}\right) K_{he}^{-0.4645+0.02303\frac{d_3}{H_3}-0.00095\left(\frac{d_3}{H_3}\right)^2}$ <p>Valid for $10 \leq \frac{d_3}{H_3} \leq 15$ and $5 \leq K_{he} \leq 25$</p>
Heat exchanger loss coefficient, K_{he} [19]	$K_{he} = \frac{2\Delta p_l}{\rho_{a34} v_{a34}^2} + \frac{2}{s_c^2} \left(\frac{\rho_{a3} - \rho_{a4}}{\rho_{a3} + \rho_{a4}}\right) + \frac{2\rho_{a4} \left(\frac{1}{\sin\theta_m} - 1\right)}{\rho_{a3} + \rho_{a4}} \left[\left(\frac{1}{\sin\theta_m}\right) + 2K_c^{0.5}\right] + \frac{2\rho_{a4} K_d}{\rho_{a3} + \rho_{a4}}$ <p>K_c and K_d are inlet contraction loss efficient and downstream loss coefficient.</p> $\theta_m = 0.0019\theta^2 + 0.9133\theta - 3.1558$ $K_d = \exp[5.488405 - 0.2131209\theta + 3.533265 \times 10^{-3}\theta^2 - 0.2901016 \times 10^{-4}\theta^3]$



Fig. 3. Finned tube heat exchanger tube bundles.

through extended surfaces or fins, as shown in Fig. 3. The convective heat transfer coefficient of air is considerably lower than that of the working fluid flowing inside the tubes, hence the surface area of the air side needs to be enhanced by a different type of fins on the bare tubes in order to accomplish the required cooling. The high pressure hot working fluid flowing inside the tubes of the heat exchanger are arranged either in inlined or staggered configuration. In many industrial air-cooled systems, circular fins and plate types of fins are employed to enhance the surface area. Fig. 4 demonstrates the terminology used for a transversal circular finned tube heat exchanger. Several individual finned tubes are arranged in a staggered or inclined configuration to form a bundle of tubes. The number of tube bundles could be from ten to hundred depending on the cooling capacity of the power plant. The staggered arrangement of tubes increases the heat transfer performance compared to the inlined arrangement. The highest temperature is limited by the fin material, the type of bonding and the material thickness.

For calculation of overall heat transfer coefficient of a finned tube heat exchanger, the following assumptions are made.

- (a) The base of the fin also conducts heat and there is no internal heat generation by the fin.
- (b) Heat transfer through fins is one-dimensional steady-state heat conduction and convection.
- (c) The thermal conductivity of the fins is constant and fins are perfectly bonded with bare tubes with zero thermal contact resistance.

The air side heat transfer and pressure drop correlations are essential for the design of finned tube heat exchanger. Briggs and Young [21] proposed the following air side heat transfer correlation applicable to finned tube heat exchanger where the tubes arranged in a staggered configuration.

$$\frac{hd_r}{k} = 0.134Pr_a Re_a \left[\frac{2(P_f - t_f)}{d_f - d_r} \right]^{0.2} \left(\frac{P_f - t_f}{t_f} \right)^{0.1134}$$

Where $Re_a = \frac{G_a d_r}{\mu_a}$

The correlation has the limits of applicability.

$$1000 < Re_a < 18000$$

$$11.013 \text{ mm} < d_r < 40.89 \text{ mm}$$

$$1.42 \text{ mm} < (d_f - d_r)/2 < 16.57 \text{ mm}$$

$$0.33 \text{ mm} < t_f < 2.02 \text{ mm}$$

$$1.30 \text{ mm} < P_f < 4.06 \text{ mm}$$

$$24.49 \text{ mm} < P_t < 111 \text{ mm}$$

Robinson and Briggs [22] correlation is used to evaluate the air side friction factor in the present analysis.

$$f_{RB} = 9.465 Re_a \left(\frac{P_t}{d_o} \right)^{-0.927} \left(\frac{P_t}{P_d} \right)^{0.515}$$

$$f_a = \frac{1}{2} \frac{D_a}{P_t} f_{RB}$$

The correlation has the limits of applicability.

$$2000 < Re_a < 50,000$$

$$18.64 \text{ mm} < d_r < 40.89 \text{ mm}$$

$$39.68 \text{ mm} < d_f < 69.85 \text{ mm}$$

$$10.52 \text{ mm} < (d_f - d_r)/2 < 14.48 \text{ mm}$$

$$42.85 \text{ mm} < P_t < 114.3 \text{ mm}$$

$$37.11 \text{ mm} < P_l < 98.99 \text{ mm}$$

$$2.31 \text{ mm} < P_f < 2.82 \text{ mm}$$

$$1.8 < P_t/d_r < 4.6$$

5. Code validation

To validate the present code, Kroger's one-dimensional model [19] of the heat exchanger is used. For the purpose of validation against the Kroger model [19], water is chosen as working fluid flowing inside the tubes of the heat exchanger. In the Kroger model, all the parameters are measured by considering the overall geometry of the heat exchanger, whereas, in the present code, a number of heat exchangers are assumed to be connected serially while the variations of the thermodynamic property of water with bulk temperature are taken into consideration. The heat exchanger unit is modelled as four tube rows and one pass. All the output parameters show very good agreement with the Kroger model under varying water inlet temperatures, as shown in Figs. 5 and 6. Table 2, shows the comparison of different parameters between present code and the Kroger model for the water inlet temperature of 40 °C and the ambient air temperature of 20 °C. Since the water properties do not change much with the bulk temperature, the Kroger model [19] is accurate to model the heat exchanger. However, this traditional method does not take account of property variations with the bulk temperature, especially for sCO₂. The validation of the present code confirms the suggested approach of sectioning the heat exchanger tube bundles. The present method of modelling the heat exchanger with sectioning allows capturing nonlinear variations of the property of sCO₂ with the bulk temperature.

Even there are numerous research studies on the modelling of various sCO₂ power cycles, but the commercially physical sCO₂ power plant is yet to build. Very few experimental studies performed on a small-scale power production (like proto-type) focused on the thermal performance of sCO₂ cycles rather than the details of sCO₂ cooling in the cooling tower. No experimental studies on the thermal performance of sCO₂ Brayton cycle coupled with the dry cooling unit are available in the literature. The only possible way for further validation of the present code is to carry out a cycle performance analysis. Wright et al. [28] at Sandia national laboratory (SNL) conducted experiments with condensing supercritical CO₂ recompression power cycle with two stages of reheating. The experiments showed improvement of thermal efficiency of a condensing sCO₂ recompression cycle over the conventional light water reactor (LWR). The cycle lower pressure was kept at 7.68 MPa, cycle pressure ratio of 1.65–2.6, shaft speed of 52,000 rpm, mass flow rate of 2.7 kg/s, turbine efficiency of 86% and a radial compressor of efficiency 66%. The two reheaters operated at 11 MPa and 15 MPa. A turbine inlet temperature of 588 K was achieved, with which a cycle thermal efficiency of 38.7% was achieved. A gas cooler was used as a cooling component and water was used as the cooling medium. In the present work, the MATLAB code is tuned for further validation with the experimental dataset provided by SNL. The present code is integrated with IPSEpro for power cycle modelling. Standard component package from this system simulation software is used and the heat transfer mechanism for the gas cooler is performed in MATLAB and water is

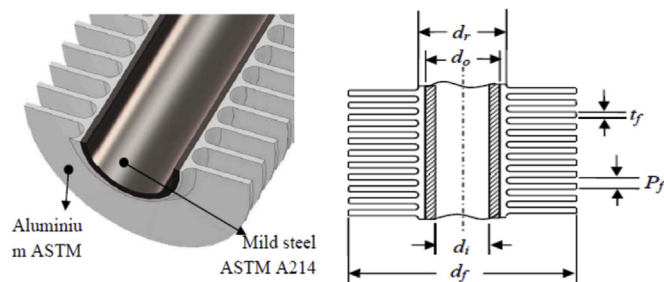


Fig. 4. Specification of different parameters of a circular fin [20].

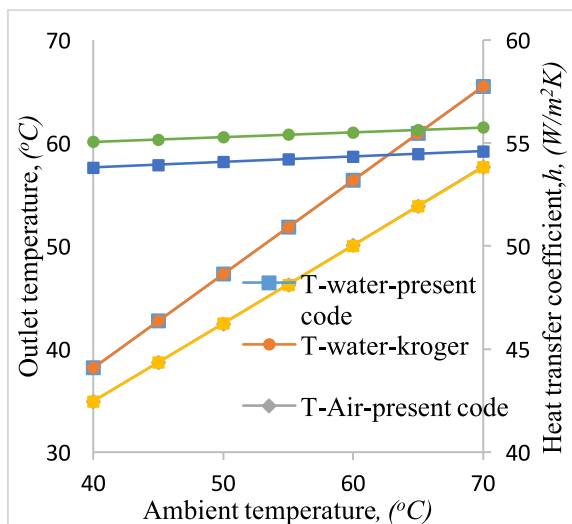


Fig. 5. Comparison of outlet temperatures and air side heat transfer coefficient between present code and Kroger model.

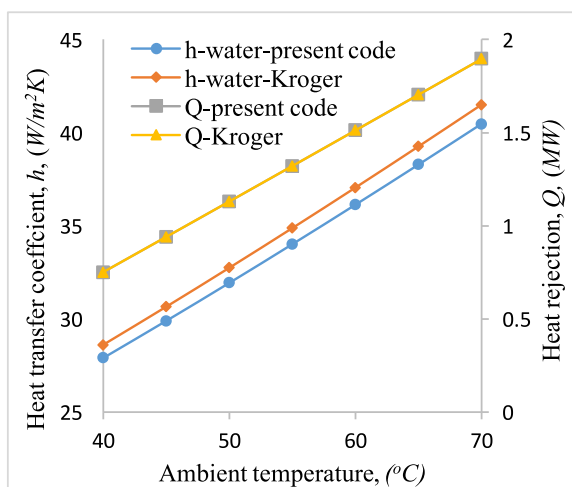


Fig. 6. Comparison of total heat rejection and water side heat transfer coefficient between present code and Kroger model.

Table 2
Code validation against Kroger model.

Parameter	Kroger model	Present code	Mean Deviation (%)
Water outlet temperature	38.2 °C	38.2 °C	0.001
Air outlet temperature	34.9 °C	34.9 °C	0.016
Total heat rejection	0.75 MW	0.75 MW	0.038
Average heat transfer coefficient of water	28615.65 W/m²K	27913.3 W/m²K	2.45
Average heat transfer coefficient of air	55.05 W/m²K	53.8 W/m²K	2.27
Water side pressure drop	53.46 kPa	53.46 kPa	0.004
Air side pressure drop	177.6 Pa	174.3 Pa	1.83

used as the cooling medium. The operating condition of the power cycle is kept same as that of SNL. In the experimental study, recuperators (HTR and LTR) effectiveness were not mentioned, hence in the present work, the values are optimized to match with experiments. Table 3, shows the comparison of the present work with SNL and present work shows good agreement with the experimental dataset.

6. Model setup and preparation

Table 4 shows the specification of heat exchanger model, where the heat exchanger is arranged horizontally and the tubes are arranged according to the staggered configuration. Each bundle contains 190 tubes, and the number of required bundles to meet the duty requirement is evaluated from the present code. The heat exchanger is modelled as four tube rows with a single pass. The design conditions are the sCO₂ inlet temperature of 71 °C, the inlet pressure of 7.5 MPa, the ambient temperature of 20 °C at atmospheric pressure of 99695 N/m². The mass flow rate of sCO₂ is determined from the plant capacity. The operating conditions of NDDCT are given in Table 5. In order to model the NDDCT, the fixed geometric parameters (Aspect ratio, tower diameter ratio, inlet height, number of tower supports, length of tower supports, the diameter of tower supports and drag coefficient of supports) are shown in Table 6. The values for various geometric parameters are taken from Kroger's [19] one dimensional model of NDDCT.

In order to evaluate the overall heat transfer coefficient for the heat exchanger, the convective heat transfer for both air side and sCO₂ are required. For this purpose, the air side heat transfer coefficient is evaluated from the most recommended Briggs and Young [21] correlation. The proposed heat exchanger model permits the use of this correlation since it satisfies all the criterion proposed by Briggs and Young [21]. The sCO₂ heat transfer coefficient is evaluated by means of Yoon et al. [29] suitable for cooling of sCO₂ in macro tubes.

$$Nu_s = a Re_s Pr_s \left(\frac{\rho_{pc}}{\rho_s} \right)^n$$

$$a = 0.14, b = 0.69, c = 0.66, n = 0 \text{ when } T_b > T_{pc}$$

$$a = 0.013, b = 1.0, c = -0.05, n = 1.6 \text{ when } T_b \leq T_{pc}$$

For the air side pressure drop calculation, the Robinson and Briggs [22] correlation is applied and the following friction factor equation proposed by Churchill [30] is used to evaluate the sCO₂ side pressure drop.

$$f_s = 8 \left\{ \left(\frac{8}{Re_s} \right)^{12} + \left[2.457 \ln \left(\frac{1}{\left(\frac{7}{Re_s} \right)^{0.9} + 0.27 \frac{\epsilon}{D}} \right) \right]^{16} + \left(\frac{37530}{Re_s} \right)^{16} \right\}^{-1.5} \frac{1}{12}$$

The properties of sCO₂ (specific heat, density, thermal conductivity, and viscosity) are measured by linking the MATLAB with the software package REEFPROP 9.0 [31].

7. Mathematical model

The extreme variation of thermodynamic properties of sCO₂ in the vicinity of the critical point is one of the key challenges associated with the modelling of NDDCT. The nonlinear variation of local heat transfer coefficient of sCO₂ with the bulk temperature close to the pseudocritical point is not predicted well by the traditional modelling of the heat exchanger. In the present code, a nodal approach is adopted to capture the drastic property variation of sCO₂ in the heat exchanger, shown in Fig. 7.

In the nodal approach, each row of tubes of the heat exchanger bundles is divided into 30 sections. Therefore, the length of each section is 200 mm. For each section, the inlet temperature of sCO₂ and air are known and the calculation starts with an initial assumption of outlet temperatures. The energy equation is satisfied for each section and the output parameters are considered as inputs for the next section. Along the length of the heat exchanger and across the tube rows, the changes of air temperature, air pressure, and sCO₂ outlet temperature are well captured by the present code. The local heat transfer coefficient and

Table 3
Validation of the various state point temperatures (K) with experimental dataset provided by SNL [28].

State Point	Experimental results by SNL [28]	Present work	Mean Deviation (%)
Entry to re-compressor compressor	295	296.3	0.44
Exit from re-compressor compressor	316.08	317	0.32
Exit from LTR of high pressure stream	428.89	433	0.94
Exit from HTR of high pressure stream	512.04	515	0.58
Exit from heat addition heat exchanger	588.15	588.15	0
Exit from high pressure turbine	559.66	560	0.06
Exit from high pressure reheater	588.15	588.15	0
Exit from intermediate pressure turbine	551.12	552	0.03
Exit from low pressure reheater	588.15	588.15	0
Exit from low pressure turbine	531.63	532	0.18
Exit from HTR of low pressure stream	432.89	435.1	0.51
Exit from LTR of low pressure stream	319.08	323.04	1.26

Table 4
Specification Heat Exchanger model.

Tube side specification			Fin side specification		
Parameter	Value	Unit	Parameter	Value	Unit
Tube material	ASTM A214 mild steel	–	Fin type	Extruded bimetallic	–
The thermal conductivity of the tube, k_t	50	W/mK	Heat exchanger arrangement	horizontal	–
Tube outside diameter, d_o	25	mm	Fin Shape	Circular	–
Tube inside diameter, d_i	20	mm	Tube arrangement	staggered	–
Relative tube surface roughness, ϵ/d_i	5.24×10^{-4}	–	Fin material	ASTM 6063 aluminium	–
Number of tube rows, n_r	4	–	Thermal conductivity, k_f	204	W/mK
Effective no. of tubes per row, n_{tr}	47.5	–	Fin diameter, d_f	57	mm
No. of tubes per bundle, n_{tb}	190	–	Fin root diameter, d_r	28	mm
Transversal tube pitch, P_t	58	mm	Fin shape	Tapered	–
Longitudinal tube pitch, P_l	52	mm	Fin tip thickness, t_{ft}	0.25	mm
Length of the finned tube, L_t	6	m	Fin thickness (mean), t_f	0.5	mm
Width of the heat exchanger	2.47	m	Fin root thickness, t_{fr}	0.75	mm
Height of the heat exchanger	0.232	m	Fin Pitch, P_f	2.8	mm

Table 5
Operating conditions of NDDCT model.

Parameter	Value	Unit
Air inlet temperature at ground level, T_{a1}	20	°C
Atmospheric pressure at ground level, P_{a1}	99695	N/m ²
Ambient temperature gradient: dT_a/dz	-0.00975	K/m
The condition of air	Dry	–
sCO ₂ inlet temperature, T_{s1}	71	°C
sCO ₂ inlet pressure, P_s	7.5	MPa
sCO ₂ mass flow rate, m_s	406.6	kg/sec
Universal gas constant, R	287.08	J/kgK

Table 6
Specified parameters for 25 MW NDDCT analysis.

Parameter	Value	Unit
The aspect ratio of the cooling tower, H_3/d_3	1.4	–
Tower inlet height, H_3	10	m
Tower Diameter ratio, d_5/d_3	0.7	–
Heat exchanger coverage of tower inlet, A_{ftr}/A_3	0.7	–
Number of tower supports: n_{ts}	$d_3/1.38$	–
Length of tower support: l_{ts}	$H_3 \times 1.15$	m
The drag coefficient of support, C_{Dis}	2	–
The diameter of tower support, d_{ts}	0.5	m

pressure drop for both air side and sCO₂ side are calculated for each small section. After calculation of the first row of tubes, the air outlet temperature and pressures are taken as input for the second row of tubes. Similarly, for all of the remaining rows of tubes, the local heat transfer and pressure drop are calculated. The present code allows for a visualization of the exact heat transfer mechanism and flow behaviour for both sCO₂ and air side along the length of the heat exchanger as well

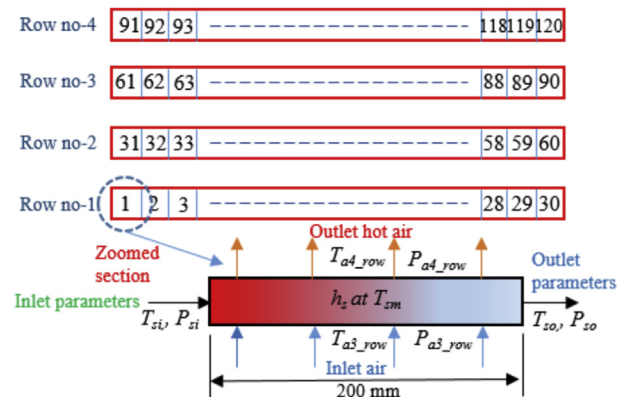


Fig. 7. An iterative nodal approach for designing air-cooled heat exchanger bundles.

as across the row of tubes.

Fig. 8 demonstrates the flow chart of simulation with the MATLAB code. The box marked with dotted line represents the calculation of parameters for each small section. All the fixed parameters in the heat exchanger and specified geometric ratios of the tower are given as inputs. With an initial assumption of air mass flow rate, M_a and mean air outlet temperature leaving the heat exchanger T_{a4} , the air pressure, temperature and density at various sections of the tower are calculated. Next, the various loss coefficients due to flow resistance encountered by the air stream are evaluated. With all these values, the draft equation is checked and if the equation is not satisfied, the air mass flow rate M_a is adjusted. The optimum air mass flow rate from the draft equation is used to evaluate the energy equation for the heat exchanger. The code starts calculation for each section with an initial assumption air outlet

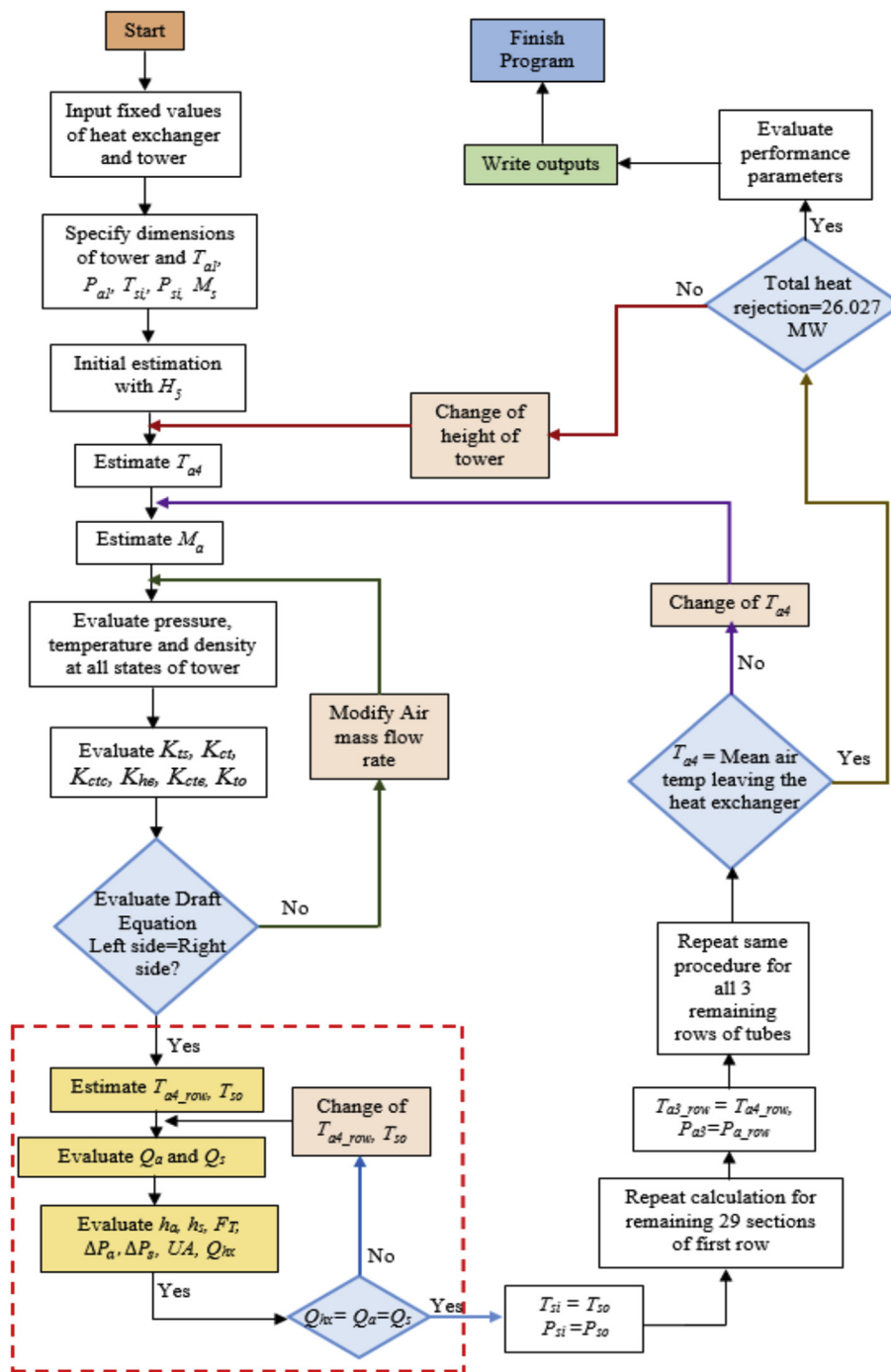


Fig. 8. Flow chart to model air-cooled heat exchanger unit in a NDDCT.

temperature, $T_{a4,row}$ and sCO_2 outlet temperature T_{so} . The outlet temperatures are modified if the energy equation for each side (air side, sCO_2 side and heat exchanger) is not satisfied simultaneously. After calculation of first section in first row, the outlet temperature and pressure (T_{so} , P_{so}) are assigned as input parameters for the next section. For all the remaining sections of first row, the same procedure is applied. For calculation of second row of tubes, the air outlet temperatures $T_{a4,row}$ and pressures $P_{a4,row}$ are assigned as inlet air temperature and pressure respectively for section number 31 to 60 of second row. Similarly, for all the remaining row of tubes, same approach is adopted. If the mean air temperature leaving the heat exchanger is not equal to the initial assumption of T_{a4} , the code modifies the air outlet temperature. The total heat rejected by the tower is the sum of heat transfer

in all 120 sections. Therefore, if the total heat rejection does not meet the tower requirements, the code modifies the tower height. The required height of cooling tower is evaluated once it satisfies the total heat rejection requirement. All the optimum parameters (tower specification, number of heat exchanger bundles and mean outlet temperatures) after calculation are shown in Table 7. Finally, the code is used with the calculated tower height to evaluate the thermal performance of air-cooled heat exchanger unit under varying operating conditions. This detailed heat exchanger model allows to control the outlet temperature of cycle fluid which significantly influences the overall cycle performance. In the present work, concentration is being paid on the design of the cooling tower and the modelling of turbo-machineries and recuperators are outside the scope of the present work. For a

Table 7

The cooling system required for a 25 MW solar power plant.

Parameter	Value	Unit
Outlet height of tower, H_5	50.622	m
Outlet tower diameter, d_5	25.31	m
Inlet tower diameter, d_3	36.16	m
Number of heat exchanger bundles, n_b	49	–
Number of tower supports: n_s	27	–
Length of tower support: l_{ts}	11.5	m
Total air side area	82,177	m ²
Total tube side area	3510	m ²
sCO ₂ mean outlet, temperature, T_{so}	40.3	°C
Air mean outlet temperature, T_{a4}	43.4	°C
Air mass flow rate, M_a	1107	Kg/sec

recompression cycle, the sCO₂ outlet temperature of the tower or the compressor inlet temperature significantly affects the cycle thermal efficiency. Using an iterative nodal approach in the heat exchanger, the cycle fluid is cooled to 40 °C. Using this value as a compressor inlet temperature, the recompression cycle with two recuperators can attain a cycle thermal efficiency of 49.2% by using a commercial system simulation software IPSEpro [32].

8. Results and discussion

8.1. Study of temperature profiles

Fig. 9 demonstrates the temperature profile of sCO₂ along the length of the heat exchanger tube bundles for each row, for the ambient air temperature of 20 °C and the inlet sCO₂ temperature of 71 °C flowing under the operating pressure of 7.5 MPa. For the first tube row, a sharp decrease of sCO₂ temperature is observed, whereas, for second, third and last tube rows, the slope of the temperature profile is less steep since the air temperature gradually rises across each tube row. This also causes the increment of outlet sCO₂ temperature at the end of each row of heat exchanger bundles. The outlet sCO₂ temperatures at the end of each row are 35.5 °C, 38.8 °C, 42.04 °C and 45.11 °C respectively. Fig. 10 shows the air temperature profile across each tube row and along the length of heat exchanger tube bundles for the same operating conditions. As the heat is transferred by hot sCO₂, air temperature rises monotonically across each tube rows. The ambient air temperature is same for the first tube row, which is reflected by a straight horizontal line. However, after air passes the first tube row, the air temperature decreases along the length of pipes. Initially, at the beginning of the tubes, the air temperature is higher than the temperature at the end of pipes since the inlet temperature of sCO₂ is high and same for each tube row.

8.2. Study of convective heat transfer coefficient

The variation of the local convective heat transfer coefficient for sCO₂ along the length of heat exchanger bundles and across each tube row is shown in Fig. 11, for an ambient air temperature of 20 °C, sCO₂ inlet temperature of 71 °C and operating pressure 7.5 MPa. As the bulk temperature of sCO₂ decreases, the local heat transfer coefficient, h_s , increases along the length of the pipe. For the first tube row, the local sCO₂ heat transfer coefficient increases significantly due to the higher temperature difference between inlet sCO₂ and ambient air. For the second, third and last row, the slope is less steep as the air temperature rises across the tube row and causes less improvement of the sCO₂ heat transfer coefficient along the length of the pipe. The average air side heat transfer coefficient, h_a across each tube row, is shown in Fig. 12. An increase of mean air outlet temperature across each tube row causes a very small increment of the air side heat transfer coefficient due to minor changes of air-side thermodynamic properties.

8.3. Study of pressure drop characteristics

Fig. 13 reveals the uniform sCO₂ pressure drop variation along the length of the pipe for each row of heat exchanger bundles. The variation of sCO₂ pressure drop at the tube inlet is more dominant due to higher Reynolds number. Along the tube length, the bulk temperature of sCO₂ gradually decreases which causes the flow Reynolds number to be decreased gradually due to increased density and viscosity at lower bulk temperature. Therefore, pressure drop decreases along the tube length and the total pressure drop at the end of each row of tubes increases essentially due to increase of the ambient air temperature. At any position along the tube length, as the row position is increased, the bulk temperature of sCO₂ increases. The increased bulk temperature provides higher values of Reynolds number due to decreased viscosity. However, in order to maintain the characteristics of the parallel flow system, the system mass flow rate is adjusted to ensure an equal pressure drop at the end of each row of tubes. The variation of air side pressure drop across the heat exchanger tube bundles is shown in Fig. 14. Air side pressure drop more or less remains constant along the tube length although, at the inlet of tubes, the pressure drop is slightly higher due to the higher temperature difference between sCO₂ and air. Air side Reynolds number and Prandtl number show minor decrease across each tube row but the thermal conductivity of air increases with temperature, which causes a slight increase of pressure drop. The total air side pressure drop is 113.16 Pa.

8.4. Study of heat rejection profiles

Fig. 15 demonstrates the sCO₂ heat rejection variation along the length of the pipe and across the tube row under the operating conditions: sCO₂ inlet temperature 71 °C, inlet pressure 7.5 MPa, ambient air pressure 99695 Pa and ambient air temperature 20 °C. Heat rejection decreases along the length of the pipe due to a gradual decrement of the temperature difference between air and sCO₂. Total heat rejected by sCO₂ for each tube rows are 8.38 MW, 6.9 MW, 5.81 MW and 4.96 MW respectively. Maximum heat rejection is obtained from the first tube rows due to the maximal temperature difference between ambient air and sCO₂.

8.5. Influence of operating pressure

The Influence of sCO₂ operating pressures (7.5 MPa, 8 MPa, and 9 MP) on the sCO₂ bulk temperatures and local heat transfer coefficients for the first tube row along the length of the heat exchanger bundles is shown in Fig. 16, for inlet sCO₂ temperature 71 °C and ambient air

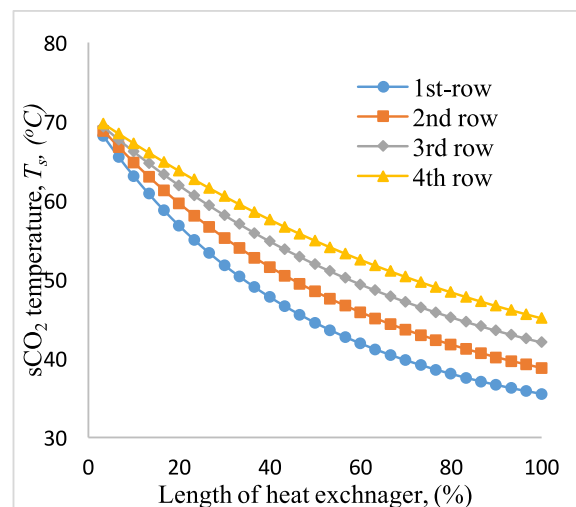


Fig. 9. sCO₂ temperatures along the length of heat exchanger bundles.

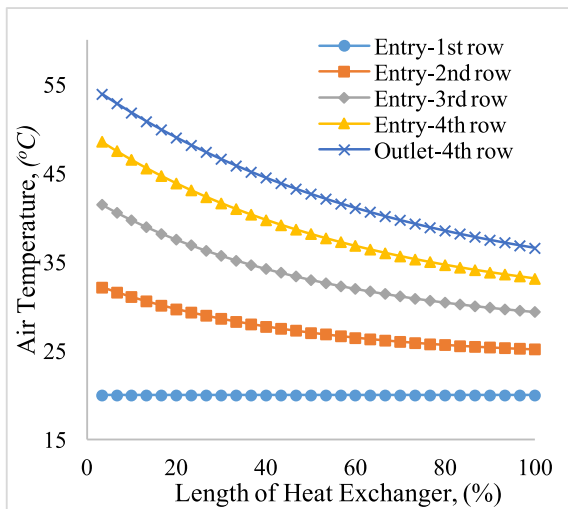


Fig. 10. Air outlet temperatures along the length of heat exchanger bundles.

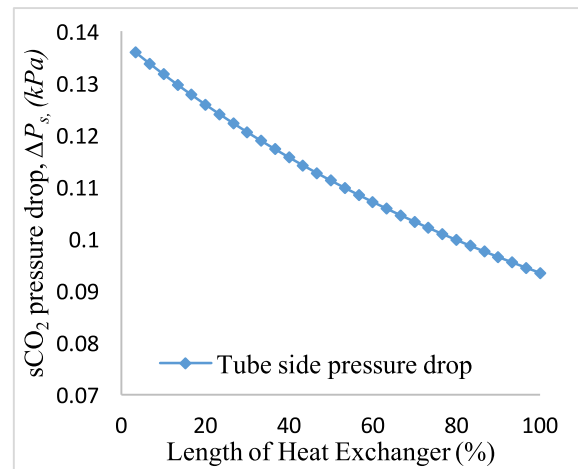


Fig. 13. sCO₂ pressure drop variation along the length of heat exchanger bundles.

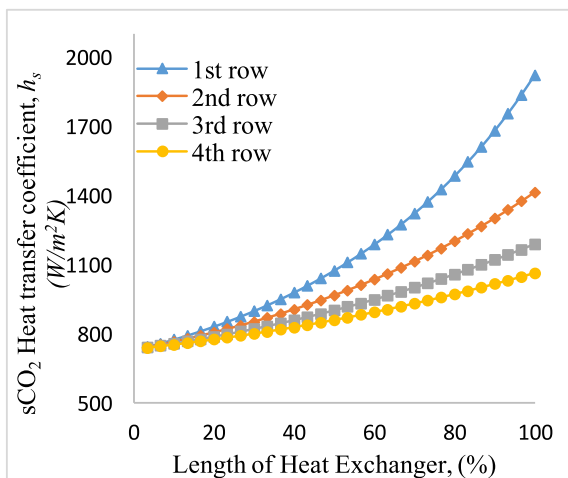


Fig. 11. sCO₂ heat transfer coefficient along the length of heat exchanger bundles.

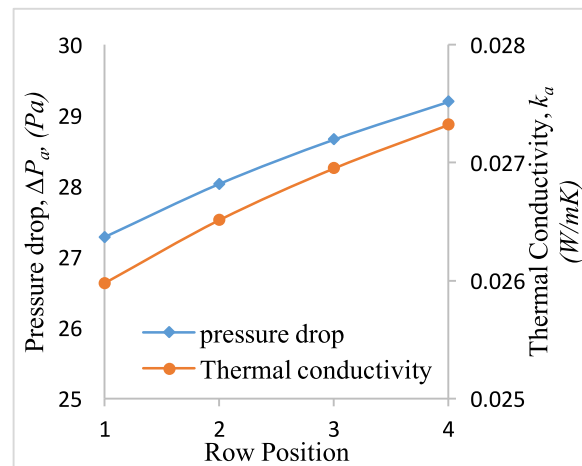


Fig. 14. Air side pressure drop across the heat exchanger bundles.

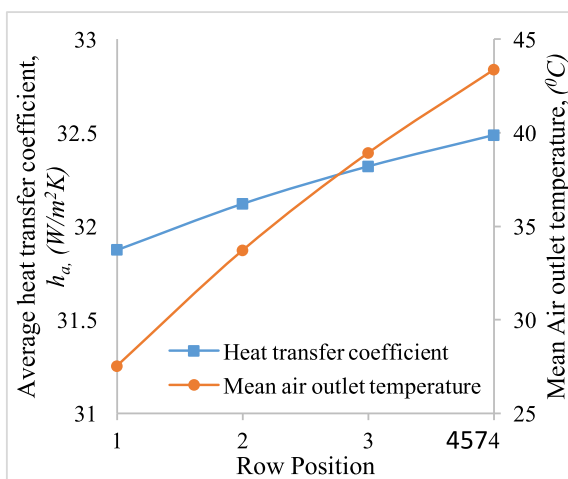


Fig. 12. Air side heat transfer coefficient across the heat exchanger bundles.

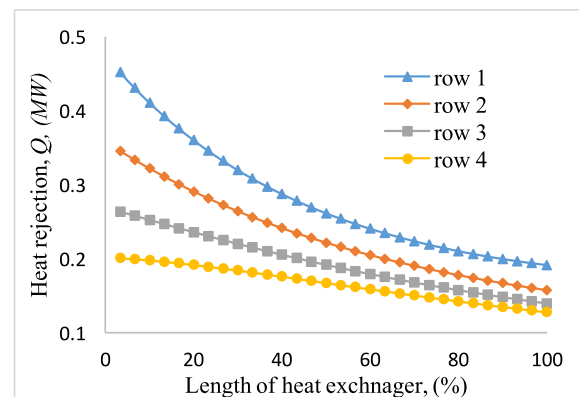


Fig. 15. Heat rejection variation along the length of heat exchanger bundles.

temperature 20 °C. As the operating pressure is increased from 7.5 MPa to 9 MPa, the outlet sCO₂ temperatures at the end of first tube row are also increased (35.5 °C, 36.5 °C and 36.86 °C respectively). A noteworthy observation of local heat transfer coefficient is scrutinised with

the increased operating pressure. For all sCO₂ pressures, heat transfer coefficient increases along the pipe length with the operating pressure with an exception for 9 MPa. The pseudocritical temperature for 9 MPa is around 39.9 °C. At tube length of 4.2 m (around 70% of the heat exchanger length), the bulk temperature of sCO₂ reaches the pseudocritical temperature, which causes a sharp increase of heat transfer coefficient due to the drastic rise of specific heat at pseudocritical temperature. When the temperature is above the pseudocritical temperature, the heat transfer coefficient decreases sharply for the

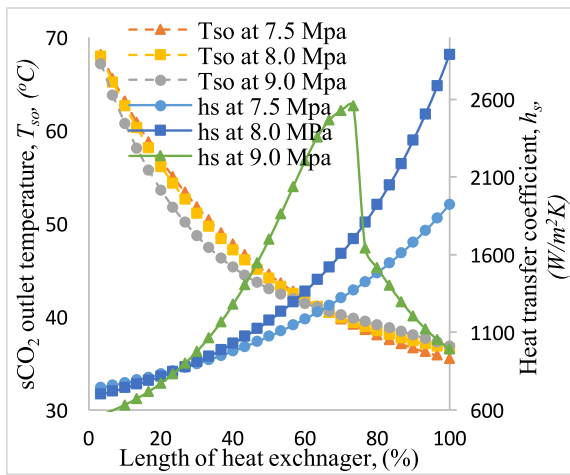


Fig. 16. Influence of sCO₂ operating pressure on outlet temperatures and heat transfer coefficient.

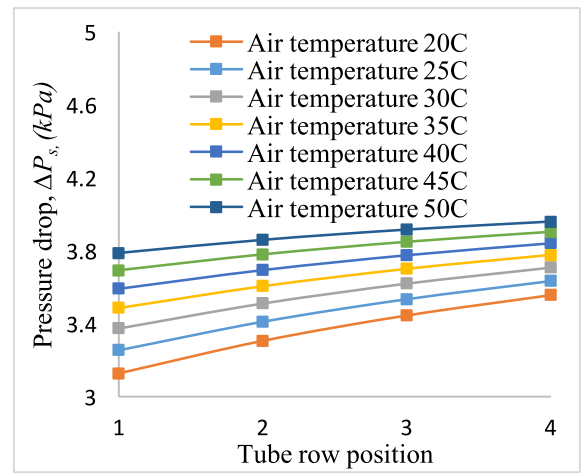


Fig. 19. sCO₂ pressure drop variation with ambient air temperature.

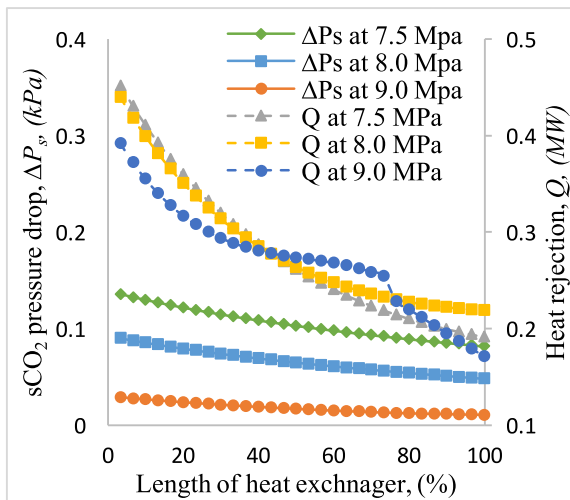


Fig. 17. sCO₂ pressure drop and total heat rejection along the length of heat exchanger bundles.

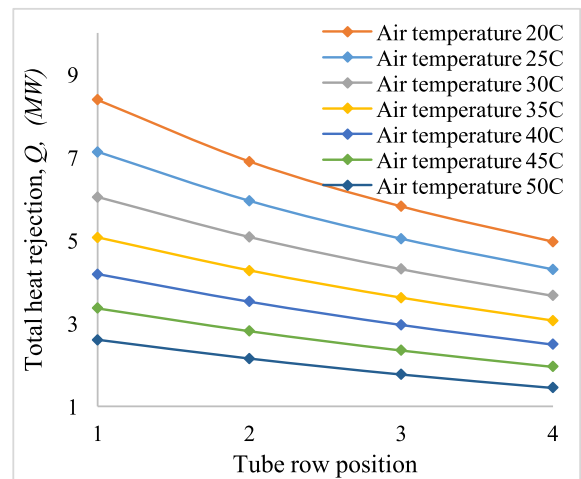


Fig. 20. Total heat rejection variation with ambient air temperature.

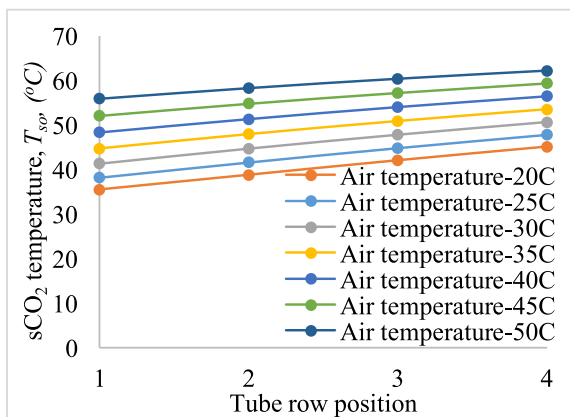


Fig. 18. sCO₂ outlet temperature variation with ambient air temperature.

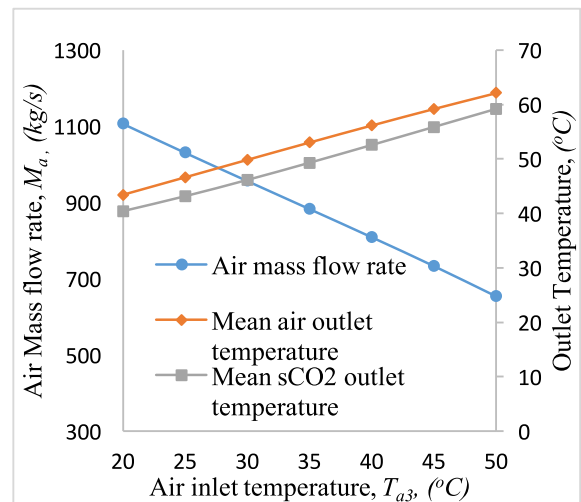


Fig. 21. Air mass flow rate and temperature variation with ambient air temperature.

remaining length of the heat exchanger tubes. For 7.5 MPa and 8 MPa, the outlet sCO₂ temperature reaches close to their respective pseudo-critical temperature (31.4 °C and 34.6 °C) at the end of the heat exchanger tubes and the heat transfer coefficient is increased with increased operating pressure.

The influence of operating pressure on the sCO₂ pressure drop and

heat rejection for the first tube row along the length of the heat exchanger bundles is investigated with an ambient air temperature of 20 °C, shown in Fig. 17. Increasing the operating pressure reduces the total pressure drop along the length of the pipe due to the smaller variation of thermo-physical properties of sCO₂ in a region further away

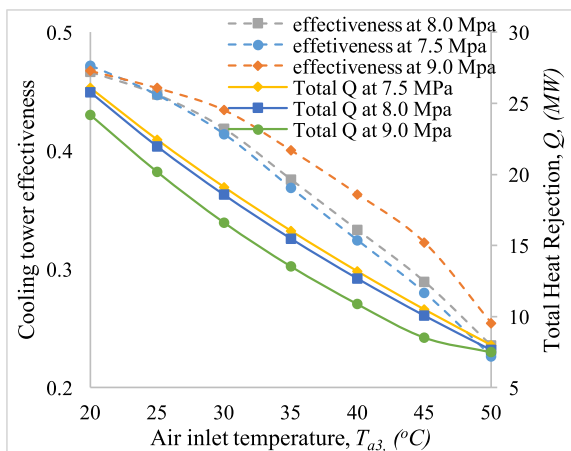


Fig. 22. Cooling tower effectiveness and heat rejection variation with ambient air temperature.

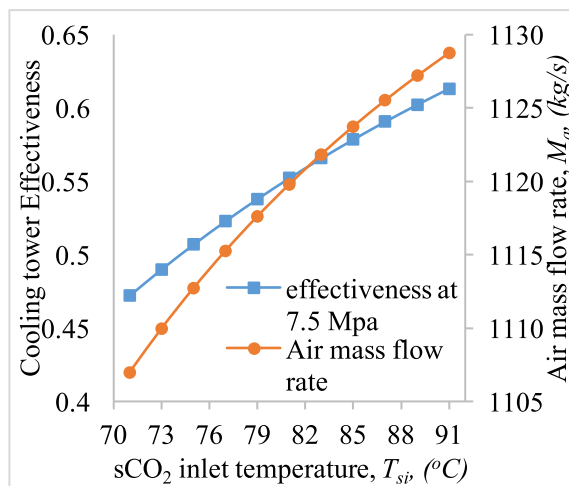


Fig. 25. Cooling tower effectiveness and air mass flow rate variation with sCO₂ inlet temperature.

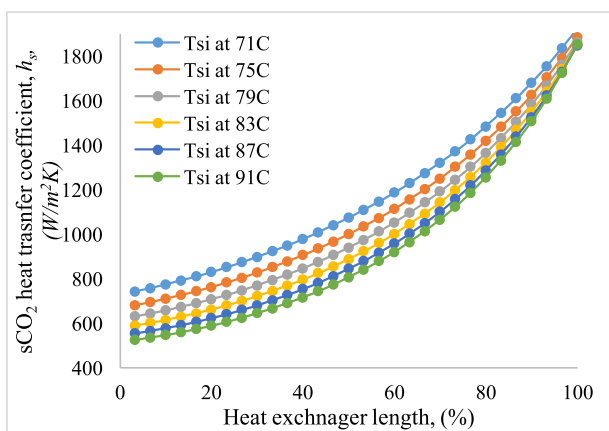


Fig. 23. sCO₂ heat transfer coefficient along the length of heat exchanger bundles.

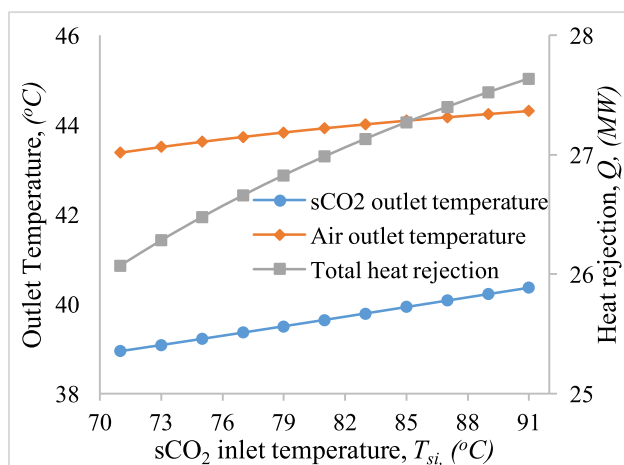


Fig. 24. Temperature and heat rejection variation with sCO₂ inlet temperature.

from the critical condition. Higher heat rejection along the length of approximately up to 40% of heat exchanger tube bundles is observed with decreased operating pressure since the sCO₂ bulk temperatures are much higher than their respective pseudocritical temperature. However, as the sCO₂ bulk temperature gradually reaches near to its pseudocritical temperature, for the remaining 60% length of heat exchanger tubes, an increase of heat rejection is observed with increased operating pressure.

8.6. Influence of ambient air temperature

The influence of ambient air temperature on the sCO₂ outlet temperature for each tube rows is shown in Fig. 18 for the inlet sCO₂ temperature of 71 °C and the inlet pressure of 7.5 MPa. As the tube row position is increased, the sCO₂ outlet temperature is also increased due to the gradual rise of air temperature across each tube rows. When the ambient air temperature increases from 20 °C to 50 °C, the sCO₂ outlet temperature also increases. The variation of sCO₂ pressure drop across the tube rows with ambient air temperature is shown in Fig. 19 under same inlet condition of sCO₂. Higher ambient temperature causes little increase of the pressure drop.

In Fig. 20, the influence of high ambient air temperature is shown on the total heat rejection under an operating condition of inlet sCO₂ temperature of 71 °C and inlet pressure of 7.5 MPa. Certainly, the heat transfer performance of the cooling tower is significantly affected during the period of high ambient temperature. For a 20 °C of ambient temperature, the total heat rejected by the tower is 26.03 MW whereas, for 50 °C of ambient temperature, the total heat rejection reduces to only 7.98 MW.

Fig. 21 demonstrates the effect of the ambient air temperature on the air mass flow rate and mean outlet temperatures of sCO₂ and air. Higher ambient air temperature considerably reduces the air mass flow rate through the cooling tower. Consequently, the total heat rejection of the tower reduces dramatically. The mean sCO₂ outlet temperature and mean temperature of air leaving the heat exchanger bundles is also increased with the increase of ambient temperature. The increase of mean sCO₂ outlet temperatures adversely affects the heat transfer mechanism in the heat exchanger.

Fig. 22 shows the trend of cooling tower effectiveness at different sCO₂ operating pressure with ambient air temperature. Higher ambient air temperature reduces the cooling tower effectiveness from 47.1% to 22.6% for an operating pressure of 7.5 MPa. Increasing the operating pressure causes an increase of mean sCO₂ outlet temperature as discussed previously. Therefore, the cooling tower effectiveness increases with operating pressure. However, this improvement of effectiveness with increased operating pressure is not justified as the total heat rejected by the tower is significantly declined with higher ambient air temperature. During the high ambient temperature period, the heat rejection capacity of the cooling tower is drastically reduced along with the cooling tower effectiveness.

8.7. Influence of sCO₂ inlet temperature

The influence of the sCO₂ inlet temperature on the local convective

heat transfer coefficient along with the length of heat exchanger bundles for the first tube row is shown in Fig. 23 for an ambient air temperature of 20 °C. For all inlet temperatures of sCO₂, the convective heat transfer coefficient increases along the length of the pipe. Increasing the sCO₂ inlet temperature slightly increases the outlet temperature at the end of the first tube row. At any position along the length of the pipe, the sCO₂ bulk temperature increases with an increase of inlet temperature. For a fixed operating pressure of 7.5 MPa, the lower the sCO₂ bulk temperature, the higher the convective heat transfer coefficient. Any lower bulk temperature approaching the pseudocritical region increases the heat transfer rate due to the dominant variation of properties near the pseudocritical region. A higher heat transfer coefficient is achieved with a lower sCO₂ inlet temperature at the same operating pressure. Although at the end of the tubes, almost the same heat transfer coefficient is observed for all range of sCO₂ inlet temperatures.

The mean outlet temperature profiles for sCO₂ and air and heat rejection with respect to the increase of sCO₂ inlet temperature is shown in Fig. 24 for the ambient air temperature of 20 °C and the inlet pressure of 7.5 MPa. The mean sCO₂ outlet temperature slightly increases with an increase of sCO₂ inlet temperature and mean air temperature leaving the heat exchanger tube bundles shows little increase in values with an increased sCO₂ inlet temperature. The heat rejected by the tower also increases from 26.02 MW to 27.63 MW for a range of sCO₂ inlet temperatures from 71 °C to 91 °C. Since the heat rejected by sCO₂ increases with inlet temperature, the cooling tower effectiveness also increases from 47.18% to 61.2% as shown in Fig. 25. The achievement of this improved heat rejection requires a higher value of air mass flow rate.

9. Conclusion

The MATLAB code developed by the authors provides the design tool for sCO₂ power plant cooling. Detailed temperature profiles and heat transfer profiles are reported by the influence of different operating parameters. The physical phenomenon behind the heat transfer mechanism and the pressure drop characteristics are also described demonstrating under various operating conditions. Higher values of local heat transfer coefficient and heat rejection are observed in the first row of tubes due to a lower bulk temperature. The sCO₂ pressure drop variation is more dominant at the entrance of tube due to higher Reynolds numbers.

The performance study is carried out for an air-cooled heat exchanger unit by varying the sCO₂ inlet temperature, pressure, and ambient air temperature. Increasing the sCO₂ operating pressure affects the heat transfer rate of the cooling system. Cooling tower effectiveness slightly increases with operating pressure but this minor improvement is not justified since the total rejection of heat by the tower decreases with increased operating pressure. During the high ambient temperature period, the cooling tower effectiveness, the heat rejected by the tower and the air mass flow rate significantly decreases with an increased ambient temperature.

Acknowledgment

This research was conducted as a part of the Australia Solar Thermal Research Initiative (ASTRI), a project supported by Australia government through the Australia Renewable Energy Agency (ARENA). The first author, M. Monjurul Ehsan would also like to acknowledge University of Queensland for providing Research Training Program (RTP) and Australian Postgraduate Award (APA) scholarships.

Appendix A. Supplementary data

Supplementary data related to this article can be found at <http://dx.doi.org/10.1016/j.ijthermalsci.2018.06.024>.

References

- [1] V. Dostal, M.J. Driscoll, P. Hejzlar, N.E. Todreas, A supercritical CO₂ gas turbine power cycle for next-generation nuclear reactors, *Proc. of ICONE*, vol. 10, 2002, p. 2002.
- [2] E.G. Feher, The supercritical thermodynamic power cycle, *Energy Conversion* 8 (2) (1968) 85–90.
- [3] Z. Ma, C.S. Turchi, Advanced Supercritical Carbon Dioxide Power Cycle Configurations for Use in Concentrating Solar Power Systems: Preprint, National Renewable Energy Laboratory (NREL), Golden, CO, 2011.
- [4] S.M. Besarati, D.Y. Goswami, Analysis of advanced supercritical carbon dioxide power cycles with a bottoming cycle for concentrating solar power applications, *J. Sol. Energy Eng.* 136 (1) (2014) 010904.
- [5] R. Chacartegui, J.M. De Escalona, D. Sánchez, B. Monje, T. Sánchez, Alternative cycles based on carbon dioxide for central receiver solar power plants, *Appl. Therm. Eng.* 31 (5) (2011) 872–879.
- [6] P. Garg, K. Srinivasan, P. Dutta, P. Kumar, Comparison of CO₂ and steam in trans-critical Rankine cycles for concentrated solar power, *Energy Procedia*, 49 2014, pp. 1138–1146.
- [7] J. Dyreby, S. Klein, G. Nellis, D. Reindl, Design considerations for supercritical carbon dioxide Brayton cycles with recompression, *J. Eng. Gas Turbines Power* 136 (10) (2014) 101701.
- [8] S.C. Yu, L. Chen, Y. Zhao, H.X. Li, X.R. Zhang, Thermodynamic analysis of representative power generation cycles for low-to-medium temperature applications, *Int. J. Energy Res.* 39 (1) (2015) 84–97.
- [9] S.-C. Yu, L. Chen, Y. Zhao, H.-X. Li, X.-R. Zhang, A brief review study of various thermodynamic cycles for high temperature power generation systems, *Energy Convers. Manag.* 94 (2015) 68–83.
- [10] T. Conboy, S. Wright, J. Pasch, D. Fleming, G. Rochau, R. Fuller, Performance characteristics of an operating supercritical CO₂ Brayton cycle, *J. Eng. Gas Turbines Power* 134 (11) (2012) 111703.
- [11] J.D. Osorio, R. Hovsapien, J.C. Ordóñez, Dynamic analysis of concentrated solar supercritical CO₂-based power generation closed-loop cycle, *Appl. Therm. Eng.* 93 (2016) 920–934.
- [12] R. Singh, S.A. Miller, A.S. Rowlands, P.A. Jacobs, Dynamic characteristics of a direct-heated supercritical carbon-dioxide Brayton cycle in a solar thermal power plant, *Energy* 50 (2013) 194–204.
- [13] R.V. Padilla, Y.C.S. Too, R. Benito, W. Stein, Exergetic analysis of supercritical CO₂ Brayton cycles integrated with solar central receivers, *Appl. Energy* 148 (2015) 348–365.
- [14] A. Conradie, D. Kröger, Performance evaluation of dry-cooling systems for power plant applications, *Appl. Therm. Eng.* 16 (3) (1996) 219–232.
- [15] Z. Zou, Z. Guan, H. Gurgenci, Y. Lu, Solar enhanced natural draft dry cooling tower for geothermal power applications, *Sol. Energy* 86 (9) (2012) 2686–2694.
- [16] K. Tanimizu, K. Hooman, Natural draft dry cooling tower modelling, *Heat Mass Tran.* 49 (2) (2013) 155–161.
- [17] D. Busch, R. Harte, W.B. Krätzig, U. Montag, New natural draft cooling tower of 200 m of height, *Eng. Struct.* 24 (12) (2002) 1509–1521.
- [18] F. Moore, Effects of Aerodynamic Losses on the Performance of Large Dry Cooling Towers, (1978).
- [19] D.G. Kröger, Air-cooled Heat Exchangers and Cooling Towers, PennWell Books, 2004.
- [20] Y. Lu, Small Natural Draft Dry Cooling Towers for Renewable Power Plants, (2015).
- [21] D.E. Briggs, E.H. Young, Convection heat transfer and pressure drop of air flowing across triangular pitch banks of finned tubes, *Chem. Eng. Prog. Symp. Ser.* 59 (41) (1963) 1–10.
- [22] K.K. Robinson, D.E. Briggs, Pressure drop of air flowing across triangular pitch banks of finned tubes, *Chem. Eng. Prog. Symp. Ser.* 62 (64) (1966) 177–184.
- [23] J. Terblanche, D. Kröger, Experimental Evaluation of the Aerodynamic Inlet Losses in Cooling Towers 10 S. Afr. Inst. Mech. Eng. R&D J, 1994, pp. 41–44 no. 2.
- [24] A. Du Preez, D. Kröger, The influence of buoyant plume on the performance of a natural draft cooling tower, 9th IAHR Cooling Tower and Spraying Pond Symposium, Brussels, 1994.
- [25] J. Geldenhuys, D. Kröger, Aerodynamic inlet losses in natural draft cooling towers, Proceedings of the 5th IAHR Cooling Tower Workshop, 1986.
- [26] A. Du Preez, D. Kröger, Experimental Evaluation of Aerodynamic Inlet Losses in Natural Draft Dry Cooling Towers, (1989).
- [27] M. Vauzanges, G. Ribier, Variation of the head losses in the air inlets of natural draft cooling towers with the shape of the lintel and shell supports, Proc. 5th IAHR Cooling Tower Workshop, 1986.
- [28] S.A. Wright, R.F. Radel, T. Conboy, G.E. Rochau, Modeling and experimental results for condensing supercritical CO₂ power cycles, Sandia Report (Jan 2011) report number SAND2010-8840.
- [29] S.H. Yoon, J.H. Kim, Y.W. Hwang, M.S. Kim, K. Min, Y. Kim, Heat transfer and pressure drop characteristics during the in-tube cooling process of carbon dioxide in the supercritical region, *Int. J. Refrig.* 26 (8) (2003) 857–864.
- [30] S.W. Churchill, Friction-factor equation spans all fluid-flow regimes, *Chem. Eng.* 84 (24) (1977) 91–92.
- [31] E.W. Lemmon, M.L. Huber, M.O. McLinden, "NIST Reference Fluid Thermodynamic and Transport Properties-REFPROP," Ed: Version, (2002).
- [32] S. IPSEpro, Process Simulation Environment (PSE), Simtech, Austria, 2003.